

Loop formation of microtubules during gliding at high density

This article has been downloaded from IOPscience. Please scroll down to see the full text article.

2011 J. Phys.: Condens. Matter 23 374104

(<http://iopscience.iop.org/0953-8984/23/37/374104>)

View [the table of contents for this issue](#), or go to the [journal homepage](#) for more

Download details:

IP Address: 24.62.200.155

The article was downloaded on 24/08/2011 at 03:39

Please note that [terms and conditions apply](#).

Loop formation of microtubules during gliding at high density

Lynn Liu¹, Erkan Tüzel² and Jennifer L Ross¹

¹ Department of Physics, University of Massachusetts Amherst, Amherst, MA 01003, USA

² Department of Physics, Worcester Polytechnic Institute, 100 Institute Road, Worcester, MA 01609, USA

E-mail: rossj@physics.umass.edu

Received 31 January 2011, in final form 28 April 2011

Published 23 August 2011

Online at stacks.iop.org/JPhysCM/23/374104

Abstract

The microtubule cytoskeleton, including the associated proteins, forms a complex network essential to multiple cellular processes. Microtubule-associated motor proteins, such as kinesin-1, travel on microtubules to transport membrane bound vesicles across the crowded cell. Other motors, such as cytoplasmic dynein and kinesin-5, are used to organize the cytoskeleton during mitosis. In order to understand the self-organization processes of motors on microtubules, we performed filament-gliding assays with kinesin-1 motors bound to the cover glass with a high density of microtubules on the surface. To observe microtubule organization, 3% of the microtubules were fluorescently labeled to serve as tracers. We find that microtubules in these assays are not confined to two dimensions and can cross one other. This causes microtubules to align locally with a relatively short correlation length. At high density, this local alignment is enough to create ‘intersections’ of perpendicularly oriented groups of microtubules. These intersections create vortices that cause microtubules to form loops. We characterize the radius of curvature and time duration of the loops. These different behaviors give insight into how crowded conditions, such as those in the cell, might affect motor behavior and cytoskeleton organization.

 Online supplementary data available from stacks.iop.org/JPhysCM/23/374104/mmedia

(Some figures in this article are in colour only in the electronic version)

1. Introduction

Biological systems have the ability to self-organize, replicate genetic information, and actively move material, and thus information, through three-dimensional space in a highly coordinated and ordered manner. While scientists and engineers have strived to shrink the scale of what they design, biology has evolved to manipulate nanoscale objects by controlling non-equilibrium processes and taking advantage of random thermal fluctuations. One specific biological system that involves self-assembly, motility, and self-organization is the cytoskeleton. The cytoskeleton is a heterogeneous network of polymer filaments within cells. It is inherently non-equilibrium, utilizing nucleotide-triphosphates in the cell to elastically form and rearrange in order to facilitate essential processes such as cell morphology change, cell motion, motor-based vesicle movement, and cell division.

Microtubules form the backbone of the cytoskeleton. They are hollow cylindrical filaments that self-assemble from tubulin subunits into a two-dimensional lattice that subsequently rolls into a tube 25 nm in diameter and are typically 1–50 μm in length. Microtubules have a persistence length of ~ 1 mm, far longer than their contour length, so they appear as rigid rods (Howard 2001, Gittes 1993, Hawkins *et al* 2010). In the cell, microtubule rigidity is harnessed to support long, extended structures such as axons, dendrites, cilia, and flagella. Microtubules have several biologically important roles. They are the support structures inside cells, as described above. They are also the tracks for long-range intracellular transport. Active transport is especially important inside the extended cellular structures that can be up to 1 m in length, because diffusion is slow over long length scales. Microtubules are also the scaffolding and mechanical elements of the mitotic spindle. The pushing and pulling of chromosomes by microtubules act

to align and separate the genetic material into two daughter cells.

The reorganization of microtubules from a radial interphase array to the mitotic spindle and back is an essential and fascinating topic for biologists and physicists alike. This procedure requires the orchestration of a large number of non-equilibrium processes and players. Thus, the general question of microtubule patterning is an important one, which has been studied in a variety of ways.

Previous work has been performed on the organization of microtubules with and without motors. Without the aid of motors, microtubules often align to form nematic liquid crystalline order *in vitro* (Guo *et al* 2007, Liu *et al* 2006, Mandelkow *et al* 1989, Needleman *et al* 2004). With the aid of associated proteins or macromolecules in solution, microtubules form bundles (Brandt and Lee 1993, 1994, Needleman *et al* 2005, Ross and Fygenson 2003, Ross *et al* 2004). *In vitro*, the bundles do not have a distinct radius, but appear stable over time. Flow can also be used to align microtubules into distinct patterns (Ross and Fygenson 2003, Ross *et al* 2004, 2008).

The first observation of microtubule patterning driven by motor proteins *in vitro* was a study showing that vesicles coated with motor proteins can drive microtubules into asters (Urrutia *et al* 1991). Further work has been performed to show that small kinesin motor complexes can form asters and vortices *in vitro* (Nédélec *et al* 1997, Surrey *et al* 2001). Asters can tile space with long-range order in hexagonal arrays, or, using two types of motor proteins with opposite polarity, square arrays are formed. Further confinement in specific geometries can lead to asters and vortex formation depending on the shape of the confining boundary.

In order to explore the self-organization of microtubules with motors, we used a simple system of the microtubule-gliding assay. In order to induce more interactions between the microtubules, we created a high density of microtubules with 3% labeled microtubules as tracers. Theoretical papers predict that, as filaments interact during gliding, they will align to form a nematic liquid crystal on the cover slip (Klumpp *et al* 2005, Kraikivski *et al* 2006). This was nicely demonstrated for actin gliding on heavy muscle myosin (Schaller *et al* 2010). We sought to test these predictions for microtubule gliding on kinesin-1 motors. As far as we know, this high-density regime has never before been experimentally examined for microtubules. In our assays, we find that the microtubules are able to pass over each other as they move, unlike the actin in gliding assays. This crossing disallowed the formation of the predicted long-range nematic organization. Short-range steric interactions cause local alignment that results in loops when locally oriented domains come into contact. Interestingly, most loops have a very small radius of curvature, which is independent of the contour length of the filament.

2. Experimental details

We purified a truncated kinesin-1 construct (Kif5b truncated at amino acid 560) with a green fluorescent protein (GFP) and 6x Histidine (6xHis) tag on the C-terminal end according to

(Pierce and Vale 1998). The sequence is in pET17b bacterial expression vector and transformed into the BL21 strain of *Escherichia coli* bacteria obtained from AddGene. We purified kinesin from 400 ml of culture induced with isopropyl β -D-1-thiogalactopyranoside (IPTG) for 12–16 h or overnight at 23 °C. Cells were harvested and lysed using freeze-thaw and sonication. His-tagged proteins were retrieved using affinity to nickel–nitrilotriacetic acid (Ni–NTA) beads (Qiagen). The protein was eluted using 500 mM imidazole. The protein viability was confirmed using gliding assays. The concentration was determined using SDS-Page gels stained with coomassie blue compared to a standard set of Bovine serum albumin (BSA) samples at known concentrations.

Tubulin was made by standard procedures and purified to 97% using a high concentration of PIPES to remove most charged associated proteins (Peloquin *et al* 2005). To polymerize and stabilize microtubules for assays, small aliquots were centrifuged at $298\,000\times g$ for 10 min at 4 °C to remove dead tubulin. The supernatant with unaggregated tubulin was incubated at 37 °C for 20 min with 1 mM guanosine triphosphate (GTP) to polymerize the microtubules. The microtubules were stabilized with 50 μ M taxol and incubated for 20 min at 37 °C. The formed microtubules were centrifuged at $14\,000\times g$ for 10 min at 25 °C, and the pellet was resuspended in 50 μ l of PEM-100 (100 mM Na-PIPES, 1 mM MgSO_4 , 1 mM EGTA, pH 6.8) with 50 μ M taxol.

To form labeled microtubules, we added 20 μ g rhodamine-labeled tubulin (cytoskeleton, Cat TL590M) reconstituted in 4 μ l of PEM-100 for 10 min to the 50 μ l of unlabeled tubulin, and then followed the protocol described above.

A typical gliding assay was performed in a flow chamber made from a slide, cover glass, and double stick tape to create a path 2–3 mm wide (figure 1). The slide and cover glass were biologically clean, and the chamber holds $\sim 5\ \mu$ l. Solution was added on one side of the chamber and removed on the other side by wicking with a Kim-wipe. The kinesin solution was added and incubated for 5 min. The chamber was then washed with wash buffer (5 mg ml^{-1} BSA, 40 μ M taxol, 20 mM DTT in PEM-100), to remove excess kinesin that did not adhere to the cover glass. Next, 5 μ l of 0.45 μ M of sheared rhodamine microtubules were incubated for 3 min. Finally, the activation mix (40 μ M taxol, 20 mM DTT, 2 mM ATP, 8.5 mg ml^{-1} glucose, 0.28 mg ml^{-1} glucose oxidase, 210 mM catalase in PEM-100) was added. Upon activation, motile microtubules were visualized with epifluorescence with a 500 ms exposure every 5 or 10 s with shuttering between frames.

For high-density microtubule-gliding assays, the chamber construction, incubation times and chamber wash remained the same as the normal gliding assay. Instead of a microtubule dilution, the microtubules were maintained at 5 mg ml^{-1} by mixing various ratios of unlabeled to rhodamine-labeled microtubules, each at 5 mg ml^{-1} (0.1%–3%). The microtubules were sheared with a Hamilton syringe 3–5 times to make the high concentration easier to pipette and to make the microtubules uniformly 5–15 μ m. The flow chamber was created as above except after incubation of the microtubules in the chamber, the chamber wash was flowed

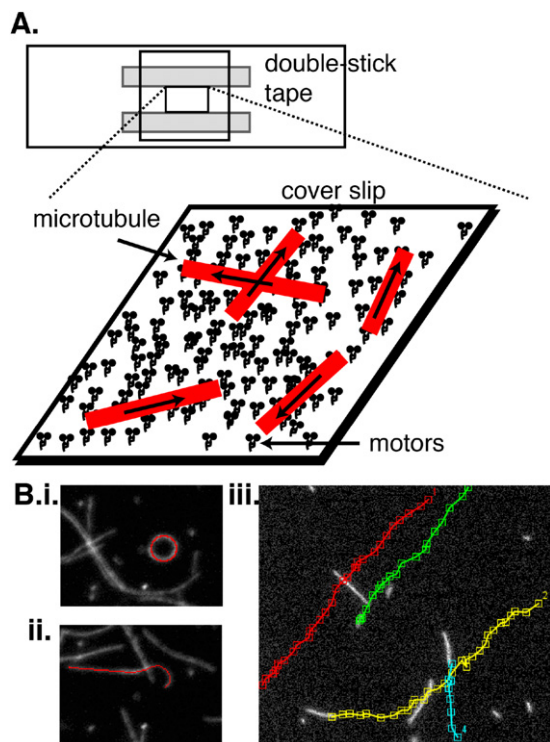


Figure 1. Experimental procedures. (A) A schematic of the flow chamber made with a microscope slide, cover slip and double stick tape with a final volume of about $5 \mu\text{l}$. Kinesin-1 motors on the surface walk toward the microtubule plus-end, pushing the microtubule minus-end forward. The microtubules can cross each other. (B) We used ImageJ to measure: (i) the radius by manual fitting of a circle and then determining the radius from the area, (ii) the filament contour length using a segmented line, and (iii) the velocity using the MTrackJ plug-in and end-tip tracking the microtubules through each frame.

through 1–5 times to reduce background fluorescence. Finally, an adjusted activation mix (the activation mix described above supplemented with an ATP regenerating system (2 mM phosphocreatine (PC); $70 \mu\text{g ml}^{-1}$ creatine phosphokinase (CPK))) was added to allow for longer imaging up to 40 min with 500 ms exposures. The time intervals between exposures were 5 or 10 s with shuttering between frames. Concentration gradients for both microtubules and kinesins were primarily accomplished with dilutions or serial dilutions into PEM-100.

Imaging was performed on a Nikon Ti-U microscope in epifluorescence using an Orca CCD (Hamamatsu) or a Cascade electron multiplier CCD (Roper). All images were exported from Nikon Elements as .tif files and then imported into ImageJ for analysis. All pixel to micron ratios are determined with a micrometer so that the $60\times$ water coupled objective yields $0.108 \mu\text{m/pxl}$. All error is the standard error of the mean (SEM) when there were high enough N -values.

The loop radius was determined by manually fitting a perfect circle to the loop curvature by holding shift and drawing with the ellipse tool in ImageJ (figure 1). Measuring the circle yielded the circle area, which was used to calculate the radius ($A = \pi r^2$). The loop duration was determined by counting the frames from start to finish, and multiplying by the time interval commencing with the first sign of curvature and terminating

when the microtubule was essentially straight again. This measurement was influenced by the microtubule length as longer microtubules took longer time to enter and leave a loop. The microtubule length was determined by manual tracing of the filament contour with a segmented line drawing tool and then measuring (figure 1). The gliding velocity was determined with the plug-in for ImageJ called MTrackJ (<http://www.imagescience.org/meijering/software/mtrackj/>) by end-tip tracking and inputting time intervals and micron distances (figure 1). The program gave an average velocity per microtubule track that was averaged over the whole movie or concentration group. N -values represent the number of microtubules tracked for each concentration. The velocity was measured on as many straight microtubules as could be visually tracked.

3. Results and discussion

We performed microtubule-gliding assays with microtubules at high densities in order to determine the self-organizational effects of the crowded landscape. We labeled a small subset of microtubules (0.1–3%) as markers for overall motion of the microtubules in the chamber. We estimate, based on the images we obtained, that the microtubules are at a density of $2.5 \text{ microtubules } \mu\text{m}^{-2}$. This value is two orders of magnitude lower than if the microtubules were close-packed rods. It is clear from the images in figure 2 that the microtubules are not close-packed. They are also not confined to the two-dimensional layer on the glass, since we frequently see crossing microtubules. Additionally, these microtubules do not appear to be bundled. We have added no cross-linkers, and the microtubules do not appear aligned enough to be influenced by van der Waals interactions.

The most striking feature of these high-density gliding assays was the increased incidence of loop formation. We define a ‘loop’ as a microtubule creating a circular profile as it glides. Numerous examples are shown in figure 2, and movies of these loops are given in the supplemental data (available at stacks.iop.org/JPhysCM/23/374104/mmedia). We measured the frequency of loop formation for high-density gliding assays and typical gliding assays (figure 3(A)). We find that loops are more than ten times as likely to form in high-density assays compared to normal gliding assays.

We believe these loops are formed due to steric interactions with neighboring microtubules (figure 2(A)). At high densities, microtubules, which are longer ($5\text{--}15 \mu\text{m}$) than they are wide (25 nm), should form liquid crystals. Indeed, this has been observed previously (Guo *et al* 2007, Liu *et al* 2006, Mandelkow *et al* 1989), and the effect can be enhanced with counterions to mask the negative surface charges (Needleman *et al* 2004), or with large polymers to enhance depletion interactions (Needleman *et al* 2005, Ross and Fygenson 2003). We believe that short-range steric interactions cause locally aligned microtubules. This is supported by the fact that many nearby microtubules are aligned in the same direction (figure 2). The misalignment is likely due to the fact that microtubules can cross each other in these assays, and are not confined to two dimensions. Thus, although there is only local

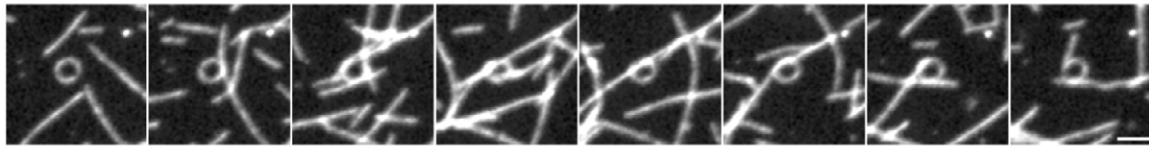
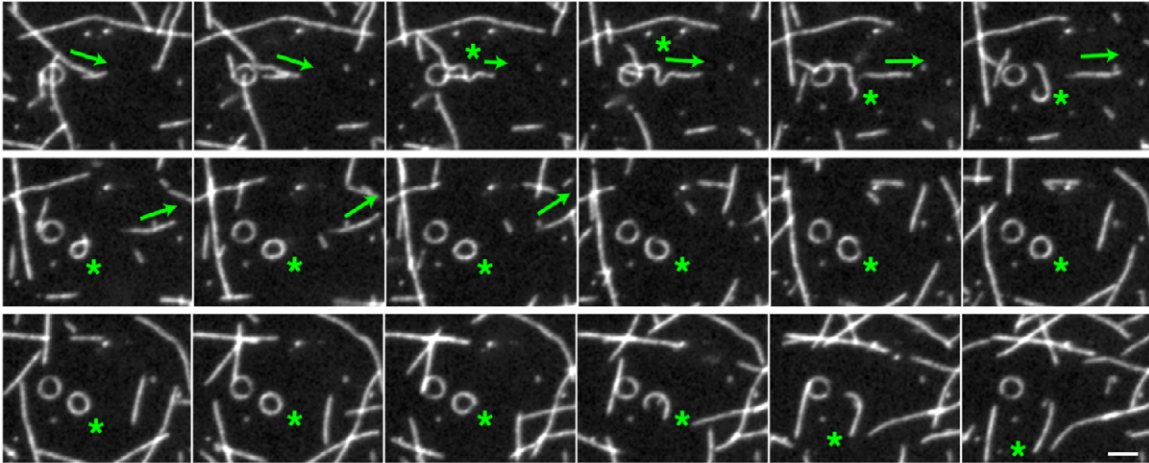
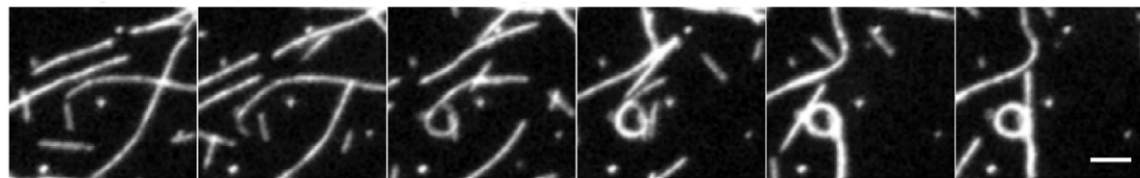
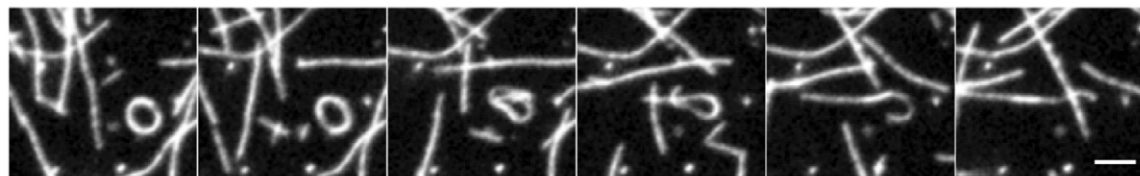
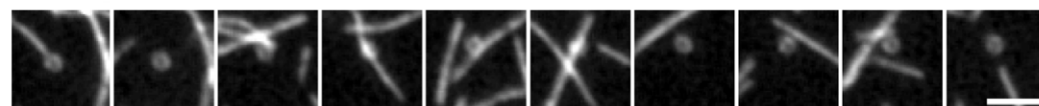
A. Loops form at “intersections”**B. Loop forming due to perpendicular forces and breakage****C. Loop forming gradually by rolling****D. Loop unrolling by deformation****E. Loops move and are not fixed**

Figure 2. Microtubule looping while gliding in crowded conditions. Chamber consists of 5 mg ml^{-1} microtubules with 3% rhodamine-labeled microtubules. Bar is $3 \mu\text{m}$ for all. (A) Microtubule loops occur more frequently at locations where other microtubules are traveling in perpendicular orientations. We call these locations ‘intersections’. The time interval between frames is 15 s. (B) Time series displaying the entire lifetime of a loop that forms through deformation and breaking of a microtubule. A microtubule traveling to the right (green arrow) comes into an intersection. Microtubules oriented vertically push the microtubule to create high bending curvature (green star). The area of high curvature breaks the microtubule into two filaments. The front end continues to the right (green arrow). The back end is pushed vertical and becomes trapped in a loop (green star). After 40 s, the loop is destabilized by intersecting microtubules and the loop unravels as the microtubule glides away to the bottom of the frame. The time interval between frames is 5 s. (C) The time series of a microtubule that forms a loop by entering it from the front. The microtubule appears to roll into the loop. The time interval between frames is 15 s. (D) Time series showing the same microtubule loop from (C) as the microtubule escapes the loop. The loop becomes deformed through the pushing of other microtubules. This deformation leads to the microtubule escaping the loop. The time interval between frames is 10 s. (E) After forming, loops migrate across the cover slip as they are buffeted by neighboring microtubules. A loop with a small radius is pushed up in this time series. The time interval between frames is 20 s.

alignment, that alignment does not persist for farther than a few microns.

What allows the microtubules to cross? Why are the microtubules not confined to two dimensions? It is likely

that our kinesin motor protein is flexible and able to stretch while staying in contact with the lattice. Previous work using high resolution imaging of gliding microtubules in the z -direction (perpendicular to the cover slip) showed that normal

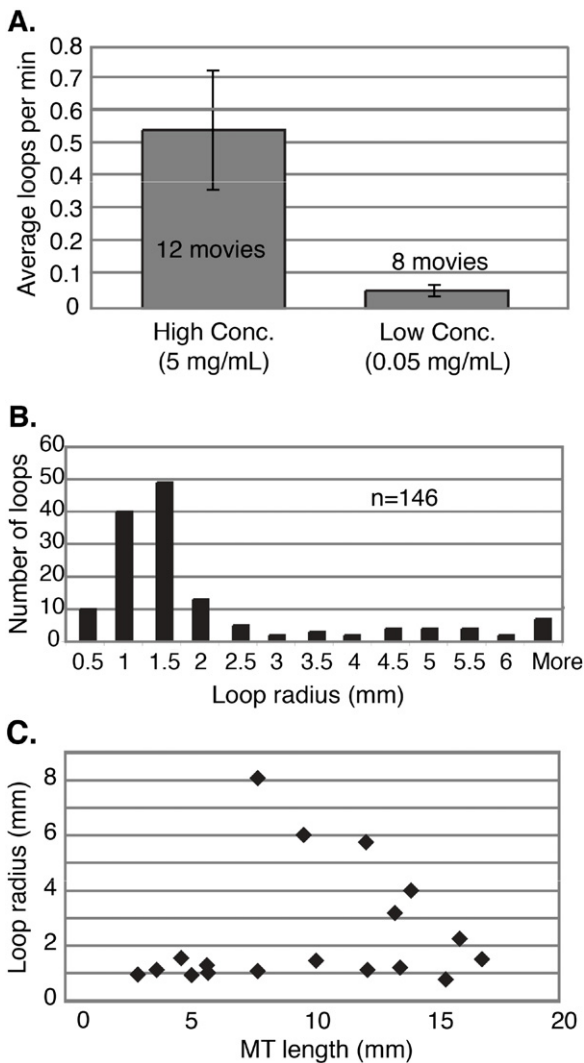


Figure 3. Characteristics of the microtubule loops. (A) Comparison of loop frequency in high concentration versus low concentration. Looping increases significantly in gliding assays with a high concentration of microtubules. (B) Histogram of the radius of the loops. Loops with smaller radii are most common ($N = 146$). (C) Loop radius versus microtubule contour length. We see two populations of microtubule radii: the first exhibits the smallest loop radius and is independent of contour length; the second displays an inverse linear dependence between loop radius and contour length.

gliding microtubules are about 75 nm from the cover glass for full-length kinesin-1 (Kerssemakers *et al* 2009). When two microtubules crossed during gliding, the height increased to 100–125 nm above the glass surface. Both microtubules continued to glide, implying that most kinesin contacts were still in place on both sides of the crossing. Thus, it is likely that the kinesin is condensed slightly during typical gliding, however when two microtubules cross, the kinesin may stretch to maximum contour length to stay in active contact with the crossing microtubule.

Because loops appear to form at locations where there are ‘intersections’ of aligned domains, we believe these microtubules are caught in the intersection. They are forced to locally align in perpendicular directions, causing them to

form a circle. Since the alignment of microtubules is local and changing, the loops are not pinned to a specific location, as evidenced by the fact that they change location (figure 2 and supplemental movies available at stacks.iop.org/JPhysCM/23/374104/mmedia). In addition, we find no preferred angle of incidence for nearby microtubules interacting with the loop (supplemental figure 2 available at stacks.iop.org/JPhysCM/23/374104/mmedia). This is not surprising considering that the angles of incidence at an intersection should include four perpendicular angles, and our intersections are rotating in the direction of the loop. Thus, over long times, all angles are sampled at the intersection location.

Our movies give us clues as to how these loops are becoming trapped at the intersection and forming. Figure 2 shows two different examples of loops forming (figures 2(B) and (C)). In the first example, a single microtubule is traversing through the intersection horizontal (green arrow). As the microtubule enters the intersection area, which is nicely denoted by a nearby microtubule loop, it is pushed perpendicular, presumably by microtubules moving vertically that are unlabeled (star). In this case, the force of the vertical microtubule is so strong that the microtubule breaks in two. The front half of the microtubule that had already traversed the intersection continues to move horizontally (green arrow), but the second half of the microtubule is pushed vertically and quickly forms a loop. The loop persists for 40 s. We observed several examples of loops being formed from breaking microtubules in our assays. A second mechanism occurs similarly, but without breaking the microtubule (figure 2(C)). In this case, the front portion of the microtubule is caught by the perpendicularly traveling microtubules, and forced to bend. The microtubule then rolls up into a loop.

Similar to formation, we observe two methods by which the microtubule can escape the loop (figures 2(B) and (D)). These are analogous to the two formation methods. The first type of escape involves a large deformation of the microtubule loop (figure 2(D)), which often takes on an ovoid shape. The deformation is likely caused by the other microtubules of the gliding assay pushing into the loop. If the deformation is large enough, the microtubule can unroll and the extended microtubule will glide away from the intersection area. The second method to escape is similar to the second method of looping. The very front portion of the looping microtubule is deformed and forced to straighten by neighboring microtubules (figure 2(B)). The microtubule is observed to simply unroll and glide away without large deformations to the loop. Although these formation and escape methods appear different, they are actually the same mechanism of steric interactions by crossing microtubules—the difference is that in one case the interaction occurs to the middle of the filament and in the other case it occurs at the tip of the filament.

In a given area, the alignment of microtubules changes over time. Further, for a given set of aligned microtubules, their alignment changes as they move in space, often rotating. We often see the location of microtubule loops shift with the change in position of the intersection of microtubules, as displayed in figure 2(E) for a small-radius loop. The movement of the loop is presumably due to the same steric interactions

with neighboring microtubules, since we observe that the loops are often pushed by nearby gliding microtubules.

We also observed high curvature microtubules being formed by pinning of the end of the filament (see for instance, supplemental movie available at stacks.iop.org/JPhysCM/23/374104/mmedia), as described previously (Bourdieu *et al* 1995, Hess *et al* 2005). This is likely due to inactive or ‘dead’ kinesin motors on the surface that transiently cross-link the microtubule to a particular position. This type of pinning is typically observed in regular, low-density gliding assays as well and can result in loop and/or spiral formation (Bourdieu *et al* 1995, Nédélec and Foethke 2007). We do not believe that the majority of the loops we observe are caused by pinning since we do not observe a position on the microtubule loop with zero velocity and loops can move around on the surface after forming (figure 2).

To further characterize the loops, we measured the radius and duration for each loop as described in section 2. The histogram of loop radius reveals that most loops have a small radius of curvature between 0.5 and 2.5 μm (figure 3(B)). For larger radii, there is an even distribution, implying that these radii are equally likely. Note that these radii of curvature are measured only for loops and not pinned microtubules.

For a subset of microtubule loops we can observe loop formation and destruction, as pictured in figure 2. For these loops, we can measure the contour length of the microtubule that forms the loops of certain sizes. We plotted the loop radius as a function of contour length (figure 3(C)). We find two subsets of microtubules: (1) one set achieves the smallest loop radii ($\sim 1 \mu\text{m}$) independent of the contour length of the microtubule; (2) the second subset have loop radii inversely proportional to the contour length. For the second subset that has decreasing loop radius with increasing contour length, a possible mechanism for this dependence is that longer microtubules have more motors and other microtubules interacting. Perhaps these additional motors and microtubules help to curl up the microtubule into smaller radii. For the subset of microtubules that always exhibit the smallest radius, perhaps they are a subset of very flexible microtubules or always have a maximal force per length acting by the motors and neighboring microtubules.

The energy to bend a filament is given by: $E_{\text{bend}} = \frac{EI}{2} \int_0^L ds \frac{1}{R(s)^2}$, where E_{bend} is the bending energy, EI is the flexural rigidity with units of energy times length, L is the contour length of the filament, s is the location along the filament, and $R(s)$ is the radius of curvature at any positions along the contour length of the filament. For our loops, the $R(s)$ is a constant for all s . So, $E_{\text{bend}} = EIL/2R^2$. If we use the persistence length, $L_p = EI/k_B T$, we have the $E_{\text{bend}} = k_B T L_p L / 2R^2$. We measured the persistence length for these microtubules and found that it is independent of length and around 0.5 mm. For the smallest loops, the radius of curvature was approximately 1 μm for all different contour lengths. We made our measurements at room temperature between 22 and 25 $^\circ\text{C}$. Using our measured parameters, we have that $E_{\text{bend}} = (2.1 \text{ pN})L$. For a 10 μm contour length microtubule, the energy to bend is $E_{\text{bend}} = 2.1 \times 10^{-17} \text{ J} = 2500k_B T$. Thus, the observed curvature cannot be caused by thermal fluctuations alone.

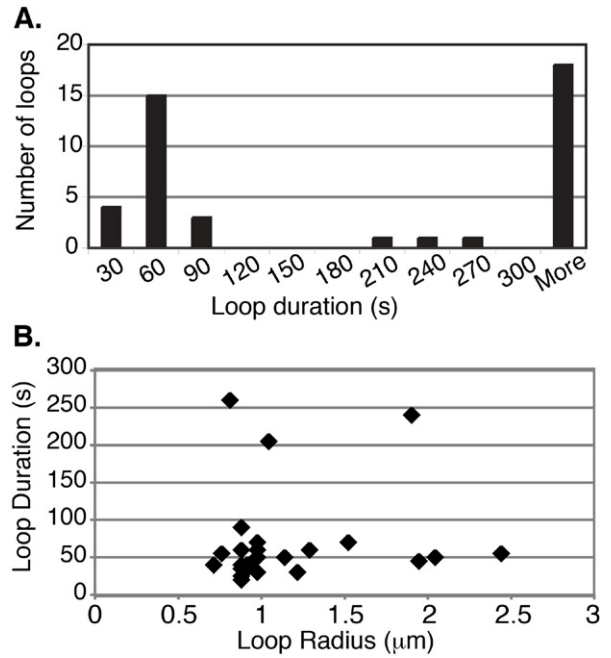


Figure 4. Persistence of microtubule loops. (A) Histogram of the duration of the loops. There are two populations of loops: those that persist for only about 1 min, and those that persist throughout the entire imaging sequence ($N = 43$). (B) Loop duration as a function of loop radius. There appears to be no dependence between loop duration and radius.

An individual kinesin motor can exert a force up to $\sim 5 \text{ pN}$ of force over an 8 nm step length, which results in the work of $E_{\text{kinesin}} = 4 \times 10^{-20} \text{ J} = 10k_B T$. Comparing these numbers, we expect that a 10 μm microtubule would require 250 kinesin motors to bend the microtubule. We estimate a maximal density of kinesin motors on the surface to be about 500 motors/ μm^2 . For a single microtubule that takes a surface area of 0.25 μm^2 , assuming the surface area of the microtubule equals the projected area ($0.025 \mu\text{m} \times 10 \mu\text{m} = 0.25 \mu\text{m}^2$), there should only be about 125 active motors on the 10 μm microtubule. Thus, we expect the steric interactions of nearby microtubules pushing on the microtubule to contribute about half of the energy required to make the smallest loops.

We also measured the time duration of loops and plotted a histogram of the loop durations (figure 4(A)). About half of the loops are already formed when the observation begins and never leave the loop throughout the entire time of imaging. In the histogram, the loops that persist throughout the movie are in the ‘more’ column on the far left. For loops we observe to form, most exist for only 30–90 s. Also, we find no correlation between the contour length of the microtubule and the duration (figure 4(B)).

The apparent trapping of some microtubules in loops may be due to the annealing of the tip of the microtubule to its end, resulting in truly formed microtubule loops. Microtubules end-to-end anneal over hours when incubated at high concentration (5 mg ml $^{-1}$). When positioned correctly in a microtubule-gliding assay, we have witnessed two microtubules annealing while being translocated. The high concentration of microtubules we use in these assays would

likely enhance the likelihood of end-to-end annealing, but may occur mostly with the unlabeled microtubules present in the chamber. For microtubules that are being forced into looping trajectories, the front and back of the microtubule would come into close proximity, and the microtubule could anneal to itself. This could only occur for microtubules where the contour length equals the circumference of the loop that is formed. The fact that these microtubules never leave the loop, the radius does not change, and that the intensity pattern stays constant throughout the imaging all imply that these loops may be end-to-end annealed. The loop featured in figure 2(A) is likely end-to-end annealed. This loop persists throughout the entire movie, and the intensity pattern along the contour is constant (although rotating). This is quite intriguing and may enable the creation of new microtubule shapes that can be studied further.

Previous studies have observed the formation of microtubule ‘spools’ created using microtubule-gliding assays and cross-linked microtubules that bundle together (Liu *et al* 2008, Hess *et al* 2005, Kawamura *et al* 2008, 2010b, 2010a). The likely mechanism of spool formation appears to be pinning of a bundle on a dead kinesin in the gliding chamber that allows for high curvature and then cross-linking of the bundle to itself (Hess *et al* 2005). Our microtubule loops are very different from the spools in several ways. First, we do not have cross-linkers in our assay, and our microtubules appear to be single, unbundled filaments based on the fluorescence intensity. Second, although we observe pinning, most loops appear to form without a pinning event to initiate looping (see figure 2). Third, our loops are much smaller than the spools observed by other groups. Our average loop radius is about 1 μm , whereas spools are typically larger 2–10 μm in radius (Hess *et al* 2005, Kawamura *et al* 2008, Liu *et al* 2008). Fourth, previous groups have found that spools form and rotate in a counter-clockwise direction (Kawamura *et al* 2010a). We find there is no preference for a specific rotation direction of our loops (supplemental figure 1 available at stacks.iop.org/JPhysCM/23/374104/mmedia), perhaps because they are being pushed by neighboring microtubules, instead of being formed through pinning, and these neighboring domains are not oriented with a preferred rotational orientation.

The flexibility of microtubules inside cells has always been difficult to measure because the strength and forces acting on the microtubules are not clear. Microtubules inside cells grow into the cell cortex and cell membrane and buckle. The buckling has been traditionally thought to be the result of compressive forces, although recent measurements show that microtubules do not bend with the curvature indicative of the lowest mode of bending (Brangwynne *et al* 2006). It has been argued that this higher mode buckling was a result of the lateral structural reinforcements provided by the surrounding cross-linked actin filaments (Brangwynne *et al* 2006).

Contrary to this finding, laser ablation studies where the microtubule was cut at the cell periphery showed that curved microtubules do not relax to straight after being cut. In fact, they did not move, but rather stayed in place with a high bending curvature (Colombelli *et al* 2005, Wakida *et al* 2007). These results imply that there is an active process keeping the microtubules in the highly curved state, and the shape is

not due to compressive loads at all. It is likely that motor proteins embedded in the actin meshwork at the cell periphery are causing these high curvature bends and actively holding the microtubules. This is reminiscent of the curvatures that occur in gliding assays when microtubules are pinned by a dead motor. This analogy between gliding assays and *in vivo* microtubule bending has recently been explored using curvature distributions of microtubules located in the periphery of LLC-PK1 epithelial cells (Bicek *et al* 2007, 2009) and in kinesin gliding assays. It was shown that microtubule curvature distributions *in vivo* and *in vitro* both exhibited an exponential decay, indicating the involvement of active forces. Thus, gliding assays, such as the ones we perform are important for determining how such motors can act to organize the microtubules.

At the cell periphery, there are fewer microtubules, which would be consistent with the normal gliding assays at low density. Areas of the cell that are crowded with microtubules, such as the cell center and in the mitotic spindle, would be consistent with our high-density gliding assays, although live cell imaging of these areas is particularly difficult and often not performed (Bicek *et al* 2009, Burakov *et al* 2003). Our assays may provide insight as to how microtubules can self-organize in dense regions of the cell in both interphase and mitosis. Future work in this area should examine the effects of different motor types, such as cytoplasmic dynein and Eg5 kinesin motors, which are both known to be major players in mitotic spindle organization (Gaglio *et al* 1996, Rusan *et al* 2002). Other interesting avenues would be to explore the effects on microtubule flexibility on the loop formation in these assays or add other factors that may modulate either the microtubules or the motors during the assay.

Perhaps the most relevant cellular system that has very high densities of microtubules is the cortical array of microtubules that wraps around the plant cell periphery (Dixit and Cyr 2004, Lucas and Shaw 2008, Shaw *et al* 2003, Yuan *et al* 1994). The microtubules in these arrays are dynamic, moving, and aligning similar to the microtubules of our high-density gliding assay. Although it is known that the microtubule motion observed in plants is due to filament treadmilling, polymerization in the front and depolymerization in the back (Shaw *et al* 2003), the *in vitro* system we created is very similar to the plant system in several ways. (1) Cortical microtubules are at very high densities as in our study. (2) Cortical microtubules ‘move’ unidirectionally like the microtubules in our study. (3) Cortical microtubules encounter each other to change orientation locally (Dixit and Cyr 2004, Yuan *et al* 1994). (4) Due to their high densities, microtubules are often observed to cross over, or co-align and bundle, and bend (Dixit and Cyr 2004). Thus, we believe that our system, and future improvements to our experimental system, may be a good *in vitro* analog to cortical plant microtubules.

Our *in vitro* studies show that, when microtubules are not well-coupled to the substrate, they do not align very well, and can form singularities, such as the loops, or ‘circulations’ we see in our experiments. This would be disastrous for cortical microtubule arrays of plants because

these microtubules play an important role in the positioning of the cellulose microfibrils. The cellulose-synthesis machinery is known to use the cortical microtubules as tracks in determining where to deposit the cellulose (Gutierrez *et al* 2009, Lucas and Shaw 2008). The chirality and orientation of the microtubules, and hence the cellulose, have far-reaching implications of overall plant chirality (Wasteneys and Ambrose 2009), and improper cellulose deposits would result in the structural failure of plants. It is therefore important to explore microtubule alignment in *in vitro* systems, particularly at high densities, to understand the mechanisms of self-avoidance, bundle formation, and the bending deformations that result in loop formations. These results will shed light on the fundamental mechanisms in which the microtubules co-align with the cell axis and the role of this alignment in growth, which is still not well understood (Gutierrez *et al* 2009).

Acknowledgments

We thank Leslie Conway for help with the purification of kinesin motors. We thank Carey Fagerstrom for the purification of tubulin proteins. This work was funded by the Armstrong Fund for Science from the University of Massachusetts Amherst to JLR, the Junior Fellows Award from the College of Natural Science (University of Massachusetts Amherst), a Commonwealth College Fellowship (University of Massachusetts Amherst), and the Howard Hughes Medical Institute Undergraduate Fellowship (University of Massachusetts Amherst) to L Liu. E Tüzel acknowledges support from the Eppley Foundation for Research.

References

- Bicek A D, Tüzel E, Demtchouk A, Uppalapati M, Hancock W O, Kroll D M and Odde D J 2009 Anterograde microtubule transport drives microtubule bending in LLC-PK1 epithelial cells *Mol. Biol. Cell* **20** 2943–53
- Bicek A D, Tüzel E, Kroll D M and Odde D J 2007 Analysis of microtubule curvature *Methods Cell Biol.* **83** 237–68
- Bourdieu L, Duke T, Elowitz M B, Winkelmann D A, Leibler S and Libchaber A 1995 Spiral defects in motility assays: a measure of motor protein force *Phys. Rev. Lett.* **75** 176–9
- Brandt R and Lee G 1993 Functional organization of microtubule-associated protein tau. Identification of regions which affect microtubule growth, nucleation, and bundle formation *in vitro* *J. Biol. Chem.* **268** 3414–9
- Brandt R and Lee G 1994 Orientation, assembly, and stability of microtubule bundles induced by a fragment of tau protein *Cell Motil. Cytoskeleton* **28** 143–54
- Brangwynne C P, MacKintosh F C, Kumar S, Geisse N A, Talbot J, Mahadevan L, Parker K K, Ingber D E and Weitz D A 2006 Microtubules can bear enhanced compressive loads in living cells because of lateral reinforcement *J. Cell Biol.* **173** 733–41
- Burakov A, Nadezhdina E, Slepchenko B and Rodionov V 2003 Centrosome positioning in interphase cells *J. Cell Biol.* **162** 963–9
- Colombelli J, Reynaud E G, Rietdorf J, Pepperkok R and Stelzer E H 2005 *In vivo* selective cytoskeleton dynamics quantification in interphase cells induced by pulsed ultraviolet laser nanosurgery *Traffic* **6** 1093–102
- Dixit R and Cyr R 2004 Encounters between dynamic cortical microtubules promote ordering of the cortical array through angle-dependent modifications of microtubule behavior *Plant cell* **16** 3274–84
- Gaglio T, Saredi A, Bingham J B, Hasbani M J, Gill S R, Schroer T A and Compton D A 1996 Opposing motor activities are required for the organization of the mammalian mitotic spindle pole *J. Cell Biol.* **135** 399–414
- Gittes F 1993 Flexural rigidity of microtubules and actin filaments measured from thermal fluctuations in shape *J. Cell Biol.* **120** 923–34
- Guo Y, Liu Y, Tang J X and Valles J M 2007 Polymerization force driven buckling of microtubule bundles determines the wavelength of patterns formed in tubulin solutions *Phys. Rev. Lett.* **98** 198103
- Gutierrez R, Lindeboom J J, Paredez A R, Emons A M and Ehrhardt D W 2009 Arabidopsis cortical microtubules position cellulose synthase delivery to the plasma membrane and interact with cellulose synthase trafficking compartments *Nat. Cell Biol.* **11** 797–806
- Hawkins T, Mirigian M, Selcuk Yasar M and Ross J L 2010 Mechanics of microtubules *J. Biomech.* **43** 23–30
- Hess H, Clemmens J, Brunner C, Doot R, Luna S, Ernst K H and Vogel V 2005 Molecular self-assembly of ‘nanowires’ and ‘nanospools’ using active transport *Nano Lett.* **5** 629–33
- Howard J 2001 *Mechanics of Motor Proteins and the Cytoskeleton* (Sunderland: Sinauer)
- Kawamura R, Kakugo A, Osada Y and Gong J P 2010a Microtubule bundle formation driven by ATP: the effect of concentrations of kinesin, streptavidin and microtubules *Nanotechnology* **21** 145603
- Kawamura R, Kakugo A, Osada Y and Gong J P 2010b Selective formation of a linear-shaped bundle of microtubules *Langmuir* **26** 533–7
- Kawamura R, Kakugo A, Shikinaka K, Osada Y and Gong J P 2008 Ring-shaped assembly of microtubules shows preferential counterclockwise motion *Biomacromolecules* **9** 2277–82
- Kerssemakers J, Ionov L, Queitsch U, Luna S, Hess H and Diez S 2009 3D nanometer tracking of motile microtubules on reflective surfaces *Small* **5** 1732–7
- Klumpp S, Nieuwenhuizen T M and Lipowsky R 2005 Self-organized density patterns of molecular motors in arrays of cytoskeletal filaments *Biophys. J.* **88** 3118–32
- Kraikivski P, Lipowsky R and Kierfeld J 2006 Enhanced ordering of interacting filaments by molecular motors *Phys. Rev. Lett.* **96** 258103
- Liu H, Spoerke E D, Bachand M, Koch S J, Bunker B C and Bachand G D 2008 Biomolecular motor-powered self-assembly of dissipative nanocomposite rings *Adv. Mater.* **20** 4476–81
- Liu Y, Guo Y, Valles J M and Tang J X 2006 Microtubule bundling and nested buckling drive stripe formation in polymerizing tubulin solutions *Proc. Natl Acad. Sci. USA* **103** 10654–9
- Lucas J and Shaw S L 2008 Cortical microtubule arrays in the Arabidopsis seedling *Curr. Opin. Plant Biol.* **11** 94–8
- Mandelkow E, Mandelkow E M, Hotani H, Hess B and Müller S C 1989 Spatial patterns from oscillating microtubules *Science* **246** 1291–3
- Nédélec F and Foethke D 2007 Collective Langevin dynamics of flexible cytoskeletal fibers *New J. Phys.* **9** 427
- Nédélec F J, Surrey T, Maggs A C and Leibler S 1997 Self-organization of microtubules and motors *Nature* **389** 305–8
- Needleman D J, Ojeda-Lopez M A, Raviv U, Miller H P, Wilson L and Safinya C R 2004 Higher-order assembly of microtubules by counterions: from hexagonal bundles to living necklaces *Proc. Natl Acad. Sci. USA* **101** 16099–103
- Needleman D J, Ojeda-Lopez M A, Raviv U, Ewert K, Miller H P, Wilson L and Safinya C R 2005 Radial compression of microtubules and the mechanism of action of taxol and associated proteins *Biophys. J.* **89** 3410–23

- Peloquin J, Komarova Y and Borisy G 2005 Conjugation of fluorophores to tubulin *Nat. Methods* **2** 299–303
- Pierce D W and Vale R D 1998 Assaying processive movement of kinesin by fluorescence microscopy *Methods Enzymol.* **298** 154–71
- Ross J L and Fyngson D K 2003 Mobility of taxol in microtubule bundles *Biophys. J.* **84** 3959–67
- Ross J L, Santangelo C D, Makrides V and Fyngson D K 2004 Tau induces cooperative taxol binding to microtubules *Proc. Natl Acad. Sci. USA* **101** 12910–5
- Ross J L, Shuman H, Holzbaun E L and Goldman Y E 2008 Kinesin and dynein–dynactin at intersecting microtubules: motor density affects dynein function *Biophys. J.* **94** 3115–25
- Rusan N M, Tulu U S, Fagerstrom C and Wadsworth P 2002 Reorganization of the microtubule array in prophase/prometaphase requires cytoplasmic dynein-dependent microtubule transport *J. Cell Biol.* **158** 997–1003
- Schaller V, Weber C, Semmrich C, Frey E and Bausch A R 2010 Polar patterns of driven filaments *Nature* **467** 73–7
- Shaw S L, Kamyar R and Ehrhardt D W 2003 Sustained microtubule treadmilling in Arabidopsis cortical arrays *Science* **300** 1715–8
- Surrey T, Nedelec F, Leibler S and Karsenti E 2001 Physical properties determining self-organization of motors and microtubules *Science* **292** 1167–71
- Urrutia R, McNiven M A, Albanesi J P, Murphy D B and Kachar B 1991 Purified kinesin promotes vesicle motility and induces active sliding between microtubules *in vitro Proc. Natl Acad. Sci. USA* **88** 6701–5
- Wakida N M, Lee C S, Botvinick E T, Shi L Z, Dvornikov A and Berns M W 2007 Laser nanosurgery of single microtubules reveals location-dependent depolymerization rates *J. Biomed. Opt.* **12** 024022
- Wasteneys G O and Ambrose J C 2009 Spatial organization of plant cortical microtubules: close encounters of the 2D kind *Trends Cell Biol.* **19** 62–71
- Yuan M, Shaw P J, Warn R M and Lloyd C W 1994 Dynamic reorientation of cortical microtubules, from transverse to longitudinal, in living plant cells *Proc. Natl Acad. Sci. USA* **91** 6050–3